ELSEVIER

Earth and Planetary Science Letters 188 (2001) 521–534

EPSL

www.elsevier.com/locate/epsl

Heat flow, sediment and pore fluid chemistry, and hydrothermal circulation on the east flank of Alarcon Ridge, Gulf of California

A.T. Fisher [a,b,*], E. Giambalvo [a], J. Sclater [c], M. Kastner [c], B. Ransom [c], Y. Weinstein [c], P. Lonsdale [c]

[a] *Earth Sciences Department, University of California, Santa Cruz, CA 95064, USA*
[b] *Institute of Tectonics, University of California, Santa Cruz, CA 95064, USA*
[c] *Geological Research Division, Scripps Institution of Oceanography, La Jolla, CA 92093, USA*

Received 10 July 2000; accepted 20 March 2001

Abstract

New seismic, heat flow, sediment and pore fluid geochemistry data from the east flank of Alarcon Ridge, at the mouth of the Gulf of California, provide evidence for vigorous hydrothermal circulation within young oceanic crust formed at a moderate-rate spreading center. Data and samples were collected 9–20 km from the ridge axis to assess the hydrologic state of 0.30–0.65 Ma seafloor. Conductive heat flow values are 15–55% of that input at the base of the lithosphere. Heat flow is highest near the center of a sediment-covered trough, and lowest along the trough margins, suggesting that trough-bounding faults and basement exposures may help to focus hydrothermal recharge. Sediment and pore fluid geochemistry data, in combination with reactive transport modeling, indicate that conditions within the shallow sediments are dominantly diffusive and reactive in two locations, but that bottom seawater recharges through the thin sediment layer with velocities on the order of 2–10 mm/yr at other sites. Seafloor heat flow appears to be entirely conductive, which is consistent with the slow rate of seepage inferred from pore fluid observations and modeling. Fluid recharge through sediments requires that basement is underpressured relative to hydrostatic conditions. We interpret these observations and inferences to indicate vigorous fluid flow in basement, and secondary seepage through overlying sediments. The heat flow deficit along the 11-km Alarcon Basin transect averages 440 mW/m^2, equivalent to heat output of 5 MW per kilometer of spreading axis. This heat output is similar to the combined focused and diffusive heat output of a single basement outcrop on the east flank of Juan de Fuca Ridge, and suggests that sites of concentrated heat and fluid outflow may exist on the east flank of Alarcon Ridge.

Keywords: hydrothermal conditions; Gulf of California; crust; heat flow; pore water; geochemistry

1. Introduction

Seafloor hydrothermal circulation results in enormous transfers of heat and solutes between oceanic crust and the overlying ocean [1]. Spec-

* Corresponding author.

0012-821X/01/$ – see front matter © 2001 Published by Elsevier Science B.V.
PII: S0012-821X(01)00310-7

tacular manifestations of this process include black smoker vents and biological communities found at ridge crests, where magma associated with crustal formation provides large driving forces. Hydrothermal circulation is also common on ridge flanks away from the spreading axis, but indications of this activity tend to be more subtle. Evidence of ridge flank circulation includes low-temperature fluid seepage and conductive heat flow values that are suppressed below, or elevated above, that expected for crust of a particular age.

While the temperatures of fluid circulation along ridge flanks are generally lower than those at the ridge crest, flank circulation results in almost 70% of the global seafloor heat flow anomaly (the difference between expected and measured heat flow) and a volume flux much larger than that associated with high-temperature ridge systems [2,3]. Because much of the seafloor has not been studied, we do not have a quantitative understanding of the distribution of hydrothermal circulation on ridge flanks, nor what processes and properties control its extent and intensity. Heat flow and geochemical data are particularly scarce from oceanic crust younger than 1 Ma, because the sediment cover necessary for penetration of heat flow and coring tools tends to be thin and incomplete.

We present results of a 1998 expedition to the Alarcon Basin at the southern end of the Gulf of California, during which swath mapping, seismic profiling, dredging, CTD casts, coring, and heat flow measurements were used to characterize the physical state of young oceanic crust. This area is particularly interesting because the young crust on either side of Alarcon Ridge records the tectonic history of the region as Baja California was split from the rest of North America and plates were reorganized over the last 5 Ma [4]. Relatively high sedimentation rates have made it possible to conduct coring and heat flow surveys over oceanic crust that is extremely young. In contrast to other spreading centers formed close to continents, Alarcon Ridge is a 'normal' mid-ocean ridge rather than a sedimented spreading center (e.g., Guaymas Basin, Gulf of California; Escanaba Trough, Gorda Ridge; Middle Valley, Juan de Fuca Ridge). Thus insights gained from Alarcon Ridge may be applicable to a large part of the mid-ocean ridge system.

2. Geological setting and previous work

Alarcon Ridge is located at the southern end of the Gulf of California and the northern end of the East Pacific Rise, just north of the Tamayo transform (Fig. 1A). Magnetic anomalies show that oceanic crust has been accreted by Alarcon Ridge since the beginning of Chron C2An (3.6 Ma), with a mean spreading rate of 50 mm/yr over the last 1 Ma [5]. Although marine geological investigations in this area date back over 30 years [6,7], the complex tectonic and geological history of the southern gulf were poorly constrained until modern swath mapping techniques, combined with magnetics profiles, seismic surveys, and improved navigation, made it possible to resolve fine-scale seafloor features.

There have been numerous heat flow studies in the central Gulf of California (e.g., [8–11]), but heat flow in the southernmost gulf is poorly resolved. Several workers [12–14] report individual heat flow values near or within Alarcon Basin (92–293 mW/m^2), including borehole measurements made during Deep Sea Drilling Project (DSDP) Leg 65. These measurements were made far from the ridge crest or across adjacent fracture zones, but the data are generally consistent with a simple $1/\sqrt{t}$ cooling model for oceanic lithosphere. These results contrast with those found in similar crustal settings of intermediate spreading rate and incomplete sediment cover (e.g., [15,16]), where heat flow is often much lower than conductive predictions. It was suggested that, south of the Tamayo Fracture zone, the high sedimentation rate may have helped to hydrologically seal the crust at an unusually young age [13]. Hydrothermal circulation in basement was inferred to be necessary to reduce seismic velocities near the base of the crust at the mouth of the Gulf of California [13], and basement is known to be hydrologically active because DSDP Hole 482C, drilled 12 km from the ridge crest through 143 m of sediments and 47 m of basalt, turned into a 'man-made hot spring' soon after drilling [17].

3. Survey design and methods

The Alarcon Basin field area was surveyed using swath mapping, magnetics, gravity, and single-channel seismic instruments during the first half of the 1998 Alarcon Basin program. We ran heat flow and coring operations based on new bathymetric maps and seismic lines that indicated the extent of sediment coverage. We focused heat flow and coring work on 0.30–0.65 Ma crust on the east flank of Alarcon Ridge, where basement structure is simply defined, and sufficient sediment cover is available for safe penetration of heat flow and coring instruments. Navigation was facilitated by a P-code differential-geographic position system in combination with dynamic positioning. This allowed coring and heat flow stations to be co-located, and subsequent seismic lines to be run immediately over heat flow and coring sites. Seismic sources were a single, 210-inch, gas injection (GI) airgun (single-channel) and a hull-mounted transducer (3.5 kHz), and the seismic survey speed was 7 kts.

Seafloor heat flow was measured using a violin-bow probe [18,19] with a 3.5-m lance that housed 11 thermistors spaced at 30-cm intervals. The instrument included a separate bottom-water thermistor and in situ thermal conductivity capabilities. Data were collected during two instrument lowerings positioned along two lines, with multiple penetrations during each lowering (Fig. 1B). Heat flow data were processed using the method described by Villinger and Davis [20]. Subseafloor depths were corrected for differences in sediment thermal conductivity through calculation of cumulative thermal resistance values, and plots of temperature versus thermal resistance (Bullard plots) were used to calculate heat flow. If conditions within the shallow sediments are conductive and at steady state, a Bullard plot will be linear, and the slope of the least-squares, best-fitting line will indicate seafloor heat flow.

Records from the shallowest thermistors commonly indicated equilibrium temperatures that deviated significantly from linear trends suggested by the deeper thermistors, probably because shallow sediments are disturbed by the weight stand above the thermistor lance [20]. We used a parameter called 'scatter' (ξ) [21] to evaluate the consistency of individual Bullard plots made with different numbers of thermistors, where $\xi = \sqrt{\chi^2/(N-1)}$, χ^2 is based on the misfit be-

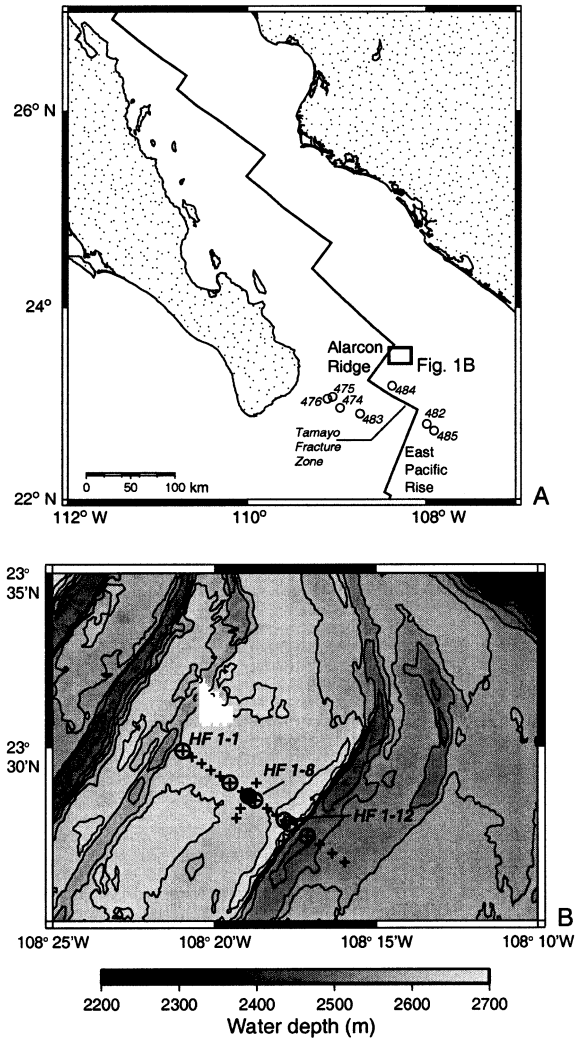

Fig. 1. (A) Southern Gulf of California and location of Alarcon Ridge. Small square is area of panel B. Deep Sea Drilling Site locations shown with open circles and numbers. (B) Swath-mapped bathymetry of east flank of Alarcon Basin, showing general structural trend running northeast–southwest. Structure curves to the northwest approaching transform to the north of the ridge. Active ridge crest is shallow region in the northwest corner of the figure. Crosses indicate locations of heat flow measurements; circles are locations where cores were collected. Labeled heat flow and core locations are discussed in the text and shown in Fig. 4.

tween equilibrium temperatures and a best-fitting straight line on a Bullard plot, and N is the number of thermistors used in the analysis ($6 \leq N \leq 11$). We favored the solution that used the largest number of thermistors by starting with $N = 11$. We calculated new values of ξ as N was reduced (by eliminating the shallowest thermistors from the analysis), and selected final heat flow values when a subsequent reduction in N did not reduce ξ. We used the range in heat flow values calculated in this way to estimate uncertainties for individual measurements (Table 1). The mean of these uncertainties is 3.0% for all stations, and the largest uncertainty is 8.6%. All values were corrected for instrument tilt ($\leq 11°$ tilt, $\leq 2\%$ correction).

The heat flow values have not been corrected for sedimentation because the sedimentation history of the basin is not known. Calculations [22,23] based on apparent sediment thickness (≤ 40 m) and crustal ages indicate corrections of $\leq 3\%$ if sedimentation was continuous since the volcanic crust was accreted (sedimentation rate = 0.06–0.1 mm/yr), or $\leq 5\%$ if all sediment accumulated in the last 100 ka (0.2–0.4 mm/yr).

Cores were collected at several sites where heat flow had been measured (Fig. 1B) using two systems: a 9-cm-diameter, gravity coring system with a 4.0-m barrel, and an eight-tube, multi-coring system capable of recovering the upper 1.1 m of sediment virtually undisturbed. Multi-core sampling allows detailed analyses of local variability

Table 1
Heat flow and coring summary from 1998 Alarcon Basin survey

Station	Pen	Latitude		Longitude		N[a]	Tilt	Q_{corr} [b]	Q_{uncert} [c]	Core type[d]	Profile type[e]
		(°N)	(min N)	(°W)	(min W)		(°)	(mW/m^2)	(mW/m^2)		
HF-1	1	23	29.899	108	20.980	11	3	133	1	MC, GC	1
HF-1	2	23	29.714	108	20.691	9	5	262	3		
HF-1	3	23	29.529	108	20.403	11	7	280	7		
HF-1	4	23	29.343	108	20.115	7	8	340	10		
HF-1	5	23	29.155	108	19.823	9	10	339	8		
HF-1	6	23	28.969	108	19.533	11	7	373	12	MC	1
HF-1	7	23	28.722	108	19.147	6	11	333	16		
HF-1	8	23	28.473	108	18.761	10	9	401	21	MC, GC	1
HF-1	9	23	28.226	108	18.376	9	7	272	13		
HF-1	10	23	28.039	108	18.086	9	7	301	5		
HF-1	11	23	27.884	108	17.839	9	5	322	4	MC, GC	2
HF-1	12	23	27.788	108	17.690	11	4	201	1	MC, GC	2
HF-1	13	23	27.436	108	17.140	11	8	255	11	MC	1
HF-1	14	23	27.188	108	16.754	11	6	194	12		
HF-1	15	23	26.940	108	16.368	10	6	147	1		
HF-1	16	23	26.692	108	15.984	10	8	164	3		
HF-2	1	23	27.956	108	19.328	9	3	253	8		
HF-2	2	23	28.231	108	19.200	10	7	304	26		
HF-2	3	23	28.507	108	19.012	9	11	322	9		
HF-2	4	23	28.534	108	18.857	9	5	357	12		
HF-2	5	23	28.598	108	18.953	9	6	427	6	MC	1
HF-2	6	23	28.660	108	19.050	7	5	402	6		
HF-2	7	23	28.688	108	18.892	10	5	378	8		
HF-2	8	23	28.965	108	18.706	8	10	380	15		

[a] N = number of thermistors used in final heat flow value.
[b] Q_{corr} = final heat flow value corrected for instrument tilt.
[c] Q_{uncert} = difference between highest and lowest heat flow value calculated using 6–11 thermistors and the final value shown in previous column; a conservative estimate of uncertainty.
[d] MC = multicore, GC = gravity core.
[e] Profile types described in the text, characteristic curves shown in Fig. 4. Type 1 profiles interpreted to indicate domination by fluid recharge; type 2 profiles interpreted to indicate domination by reaction and diffusion.

of chemical and physical properties. Both systems recovered sediments in butyrate tubes.

After being brought on deck, cores for pore water analyses were immediately capped, taped and taken to a cold room (4–9°C) for processing. Cores for physical properties were sampled immediately on deck and those for organic carbon analyses were frozen until analyzed on shore.

Cores collected for pore waters were sectioned in a nitrogen glove bag at discrete depth intervals and samples were immediately placed in centrifuge tube and spun in a refrigerated ultracentrifuge to separate the sediment and pore water. Pore waters were then extracted from the sample tubes in a nitrogen-filled glove bag and aliquots were immediately analyzed for alkalinity (by titration) and ammonium (by spectrophotometry), and tested for sulfide (precipitated as CdS). The remainder of each sample was sealed in glass ampoules and archived for analysis of other chemical components in the onshore laboratory.

Sediment water content and porosity were determined by sampling known volumes of sediment and comparing wet and dry masses; dry masses were corrected for salt content prior to porosity determinations. Because of the high water content of the surface sediments, the uncertainty of these measurements was probably ±5% in the upper 5 cm, but decreased to ±2% with depth.

The total organic carbon content of the sediment was determined, by difference, using total carbon data from a Perkin-Elmer CHN Analyzer and data for carbonate obtained from a coulometer. Different aliquots of the same finely ground, freeze-dried sample were used for both methods. Precision of analyses, as determined by repeated measurements of the same sample, was ±2%.

4. Heat flow and seismic results

The first line of heat flow measurements and sediment cores was oriented parallel to the spreading direction and perpendicular to primary seafloor structure, forming a transect 9–20 km from the active ridge (Fig. 1B). The transect crossed a sediment-covered trough 7 km wide, then continued over the adjacent abyssal hill towards the southeast. A second line of heat flow measurements and cores was run down the center of the trough perpendicular to the first line, parallel to the overall structural trend (Fig. 1). The trough is bounded to the northwest and southeast by abyssal hills rising 40–80 m above the adjacent seafloor. This is the third trough southeast of the ridge, and the first within which smooth bathymetry and seismic data suggested that sediment cover was continuous.

Shallow sediment thermal conductivities varied linearly with depth from 0.70 W/m°C near the seafloor to 0.85 W/m°C at 4.5 m below the seafloor (mbsf) (Fig. 2A). Seven conductivity measurements near 3.0–3.5 mbsf indicated higher conductivities, 0.9–1.2 W/m°C, probably indicative of a sandy (turbidite?) layer. Because this higher-conductivity layer was not measured during all penetrations, it must be discontinuous or thinner than the 30-cm thermistor spacing of the heat flow lance.

All heat flow measurements are consistent with conductive, steady-state conditions in shallow sediments, and values vary from 133 to 427 mW/m^2 (Table 1; Figs. 2–4; Bullard plots for all measurements are available at: emerald.ucsc.edu/~afisher/alarcon). The highest values are found near the center of the trough, and there are locally elevated values over the abyssal hill near the southeast end of the first heat flow line (Figs. 3 and 4). Conductive heat flow in the survey area is 15–55% of that input at the base of the lithosphere for crust of this age (Fig. 4), suggesting that much of the heat loss in this area is advective. Heat flow is lowest at the trough margins immediately adjacent to the edges of abyssal hills.

Seismic lines run along the first heat flow and coring transect (profile L–L′) illustrate gross sediment and crustal structure, including several notable features (Fig. 4). Sediment thickness estimated from the single-channel seismic line is relatively constant within the main trough (0.05 s-twt, about 37 m), but thins over the hills to either side of the trough. Sediment may be thicker locally near the edges of the trough where basement appears to deepen (Fig. 4). Picking sediment thickness from these records is difficult near the edges of the abyssal hills because of side echoes.

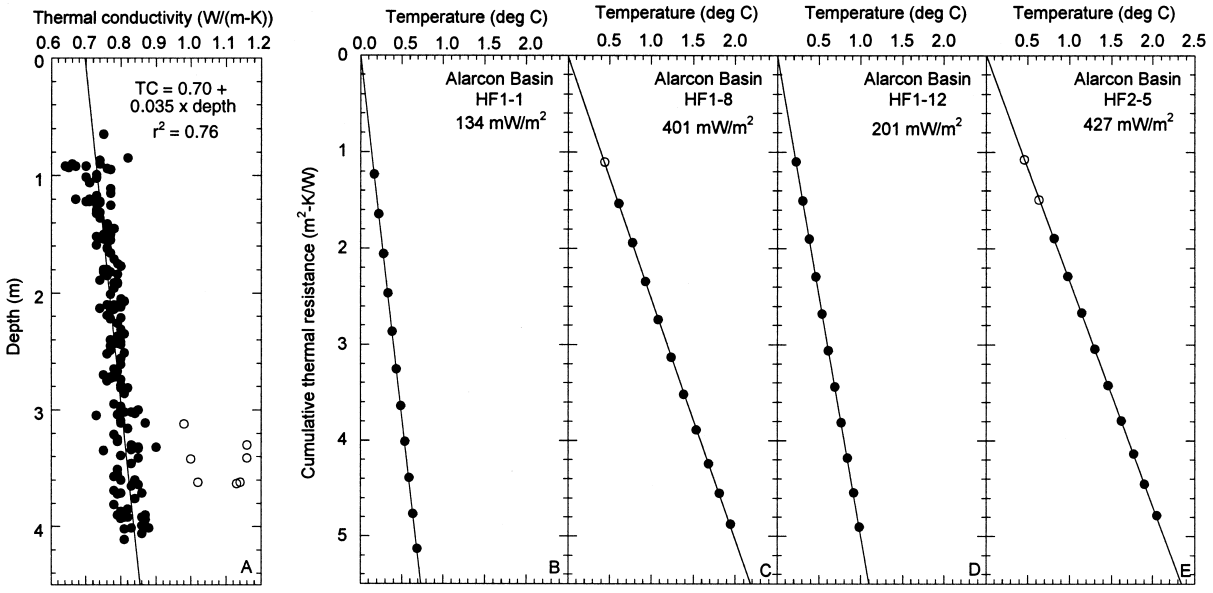

Fig. 2. Thermal conductivity and example Bullard plots (temperature versus cumulative thermal resistance) from the 1998 Alarcon Basin survey. Temperatures are plotted as deviations from bottom water values, and depth-shifted so that the best-fitting line (slope = heat flow) passes through 0°C at the seafloor. (A) In situ thermal conductivity data from all measurements. Filled circles indicate measurements used to generate the linear thermal conductivity versus depth function shown with a solid line. Open circles indicative of locally elevated thermal conductivity at 3.0–3.5 mbsf were omitted from the function fit. (B) Bullard plot of station HF1-1. All 11 thermistors used in heat flow calculation. (C) Bullard plot of station HF1-8. The shallowest thermistor (open circle) was omitted from heat flow calculation (as described in the text). (D) Bullard plot of station HF1-12. All 11 thermistors used in heat flow calculation. (E) Bullard plot of station HF2-5. The shallowest two thermistors (open circles) were omitted from heat flow calculation (as described in the text).

The 3.5-kHz records reveal coherent sedimentary layering within the trough and over the top of the abyssal hill to the southeast (16–18 km from the ridge axis). Temperatures within uppermost basement calculated from the measured heat flow and sediment thicknesses estimated from the seismic records are 5–20°C. The lowest apparent basement temperatures are associated with low heat flow and thick sediments at the edges of the trough (HF1-1 and HF1-12; Fig. 4).

Narrow (300–500-m-wide) zones of acoustically transparent sediment are apparent on both 3.5-kHz and single-channel seismic records (Fig. 4). There is continuity of the shallowest layers within these zones, but layering becomes less distinct with depth and disappears entirely near basement. A crossing line run parallel to basement structure along the second heat flow transect indicates that these features are spatially restricted and approximately circular in plan view.

Similar sediment structures were noted along a shallow, buried basement ridge on 1.0 Ma crust east of the Juan de Fuca Ridge using GI gun, water gun, and Parasound (4-kHz) records. These structures were interpreted to indicate elevated sediment porosity and an associated reduction in seismic impedance [24]. Pore fluids squeezed from cores in that area indicated that fluid was seeping from the seafloor at about 2 mm/yr (Ocean Drilling Program (ODP) Sites 1030 and 1031 [25]). Zühlsdorff et al. [24] hypothesized that fluid flow had altered sediment properties, and that the characteristic seismic signature could be used to infer locations of seafloor seepage. Sedimentological and geotechnical tests of sediments from the Juan de Fuca flank seepage area demonstrated that porosities and permeabilities were elevated relative to those at similar depths at nearby sites [26], but also indicated that differences in properties could be explained entirely by differences in

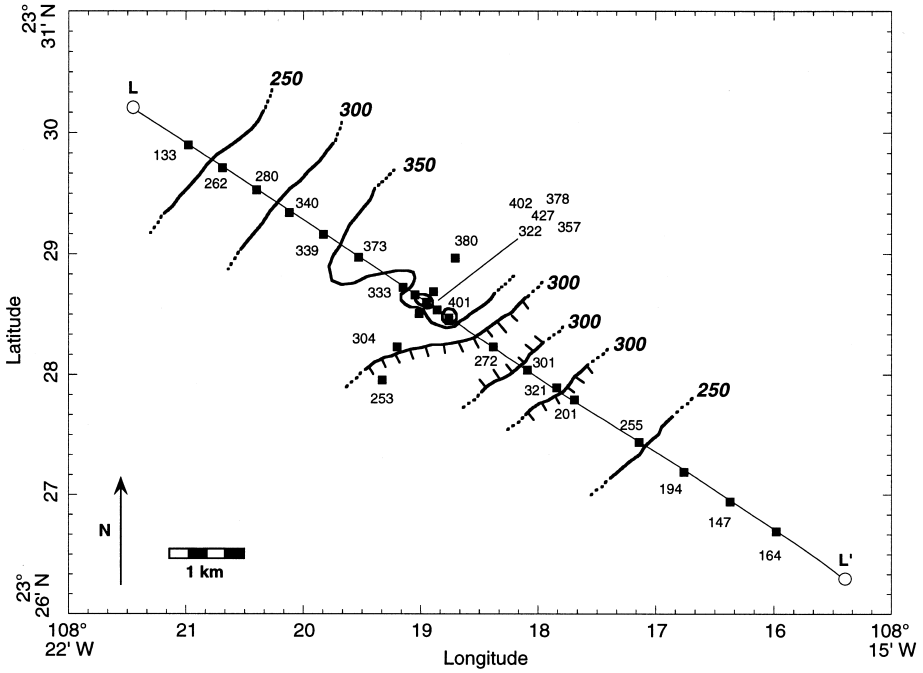

Fig. 3. Heat flow values (mW/m^2) and hand-drawn heat flow contours (50 mW/m^2 interval). L–L′ indicates track for seismic lines and heat flow profile shown in Fig. 4.

primary lithology. Hemipelagic clay, which would be deposited preferentially over topographic highs, tends to retain its initial porosity to greater depths than do the fine-grained turbidites, which tend to be deposited in lower-standing areas. Variations in seafloor elevation of only a few tens of meters could result in a spatial differences in deposition of these distinct sediment types.

Although the single-channel seismic records from Alarcon Basin do not allow an unequivocal assessment of local basement topography, there appear to be small basement highs below several of the transparent zones (Fig. 4C). In addition, swath maps of the unsedimented crust close to the ridge crest reveal numerous circular, volcanic features dotting the seafloor, with topographic relief of 20–100 m and diameters up to several hundred meters. These features are more common along the west flank of Alarcon Ridge, but are present along the east flank as well. For this reason, and because the pore fluid data (described below) are most consistent with diffusive, reactive, and slow hydrologic recharge conditions within the shallow sediments, we suggest that small basement highs may be responsible for the narrow zones of acoustically transparent sediment. One explanation is that basement highs accumulate finer-grained hemipelagic sediments than does the surrounding seafloor, as observed on the Juan de Fuca Ridge flank. A variation on this interpretation is that small basement highs result in sediments that are sufficiently tilted so as to disrupt seismic layering. In either case, when the relative magnitude of topographic relief is reduced, following initial sedimentation, more continuous layering is established across these basement highs (Fig. 4). Detailed seismic, coring, and geotechnical work will be required to test applicability of these hypotheses to the east flank of Alarcon Ridge.

5. Sediment and pore water results

Sediments recovered by coring in Alarcon Basin are mainly hemipelagic mud. Mineral X-ray dif-

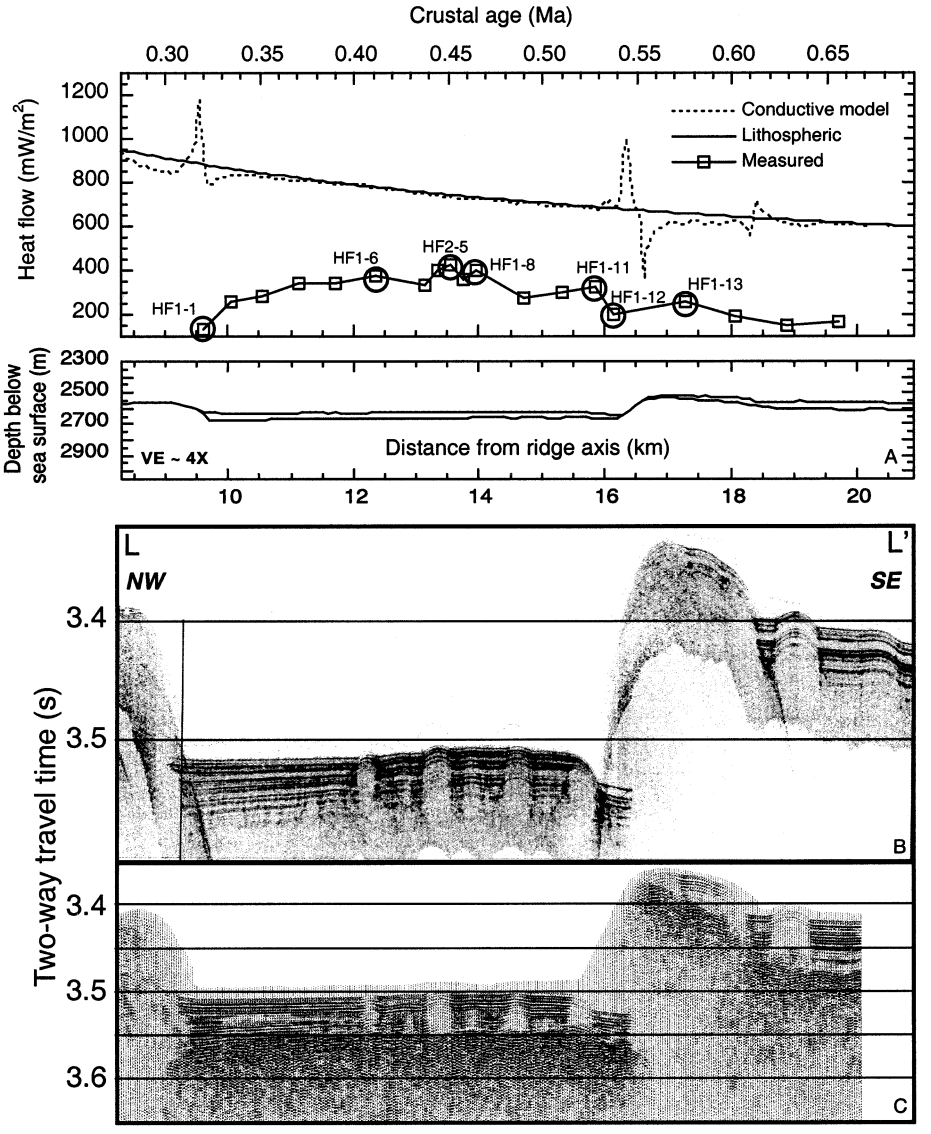

Fig. 4. (A) Measured heat flow values (open squares) along profile L–L′. Solid curve is expected heat flow based on crustal age [2]. Dashed line is conductive seafloor heat flow from a numerical model. Conductive model was based on layering of sediments and basement interpreted from seismic profiles, as shown in the line drawing. Line drawing is vertically exaggerated by 4∞. The conductive solution was calculated using a constant bottom water temperature, heat flow in at the base of the system varying with crustal age, and appropriate sediment and basement thermal conductivity values. Circles indicate locations where cores were collected. (B) 3.5-kHz profile along line L–L′ (Fig. 3), perpendicular to strike of primary tectonic features. Note narrow zones of acoustically transparent sediment. (C) Single-channel seismic record along line L–L′, used to pick seafloor and basement depths and create the finite-element grid used for the conductive model.

fractograms and organic carbon (OC) analyses indicate that surface and near-surface sediments are compositionally similar throughout the study area. Sediment carbonate contents are generally low (~0.3 wt%), with slightly elevated values (0.4–0.6 wt%) found throughout the cores, and values up to 2.0 wt% occurring near 2 mbsf at HF1-1 (Figs. 1B and 4). OC contents are gener-

ally uniform and relatively high, 4.0–4.5 wt% in the first 2 m of sediment, except at HF1-12 (Fig. 1), where values are 0.5–2.0 wt% lower. These differences could have resulted from local variations in the deposited proportions of hemipelagic sediment, perhaps resulting from winnowing of fine-grained sediments along the edge of the sedimented trough (Fig. 4).

Given the small size of the area investigated (Fig. 1B) and the similarity of sediments recovered along the transect, pore water profiles across the trough were expected to reveal similar geochemical characteristics. Because the recovered sediments exhibited high OC contents, we anticipated measuring large gradients in pore water alkalinity, ammonium, and sulfate related to the bacterial degradation of organic matter.

Concentration–depth profiles of Alarcon Basin pore waters can be classified into two groups that we have designated 'type 1' and 'type 2' profiles (Fig. 5). In type 1 profiles, the concentrations of pore water species analyzed do not deviate, or deviate only slightly, from those of bottom seawater. In contrast, type 2 profiles show evidence of significant diffusion and water–sediment reaction. Differences between the two groups are particularly striking for ammonium, alkalinity, sulfate, and calcium concentrations, all of which are influenced by the bacterially mediated decomposition of sedimentary organic matter. The only two sites with type 2 profiles are HF1-11 and HF1-12 at the southeast edge of the trough (Table 1, Fig. 4A).

The most probable causes for the observed deviations in geochemical behavior are differences in microbiological reactions, temperature, and hydrologic regime. The first possibility can be discounted on the basis of: (1) the observed compositional and sedimentological homogeneity, and (2) the short distance (1.2 km) between stations that exhibit strong biologically mediated organic matter degradation (type 2) and those showing little biological activity (type 1). Interestingly, the type 1 site that shows the weakest geochemical indication of bacterial activity (HF1-8) has a higher OC content (4.0–4.5 wt% in the upper 2 mbsf) than does the type 2 site that shows the strongest evidence of bacterial activity (HF1-12; the OC content is 3.7 wt% at the top of the core and gradually decreases to 2.4 wt% at the core bottom).

There are only small differences in sediment temperatures between the various sites. With maximum sediment thicknesses ≤ 40 m and heat flow suppressed well below lithospheric values throughout the study area (Figs. 3 and 4), temperatures at the top of basement are ≤ 20°C, too low to cause significant thermal degradation of buried organic matter.

The explanation we prefer for the observed contrast in pore water gradients along the transect is that differences in hydrologic regime either mask (type 1) or fail to mask (type 2) reactions within the shallow sediments. Type 1 profiles are attributed to seawater downwelling that erases the consequences of reaction, while type 2 profiles indicate a lack of seawater downwelling. In Section 6 we describe how hydrothermal circulation in basement may lead to secondary recharge through shallow sediments, and estimate the minimum recharge velocities required by the pore water profiles.

6. Alarcon Basin hydrogeology

6.1. Geothermal analyses

If heat loss along the Alarcon Basin transect was entirely conductive, seafloor refraction would lead to elevated heat flow at the edges of abyssal hills, and locally lower values over seafloor highs (e.g., [27]). To quantify the magnitude of conductive refraction, we prepared a two-dimensional numerical model that includes basement relief, sediment thickness, and sediment and basement thermal conductivity values (Fig. 4A). Heat input at the base of the model varied with crustal age. Because of refraction and the pinching out of sediments at the edges of basement outcrops, modeled conductive heat flow tends to be sharply elevated along the edges of the sediment-filled trough and relatively low over the basement high 16–18 km from the ridge crest. In contrast, the greatest measured heat flow values are found near the center of the trough, and there is locally

elevated heat flow over the basement high to the southeast. The lowest heat flow values were measured at the base of abyssal hills on either side of the trough, suggesting that faults associated with these feature may help to focus recharge of cold bottom water. Slightly elevated heat flow over the basement high 16–18 km from the ridge (Fig. 4) may indicate local advective redistribution of heat within basement beneath this feature.

We assume that there is a component of across-strike fluid flow within basement, with fluid entering the outcrop northwest of the heat flow transect and flowing to the southeast, and use an analytical model of coupled heat and fluid flow [28,29] to estimate the lateral specific discharge (volume flux per unit area) required to explain the observed suppression in heat flow. Assuming a 40-m-thick sediment layer, a 500-m-thick perme-

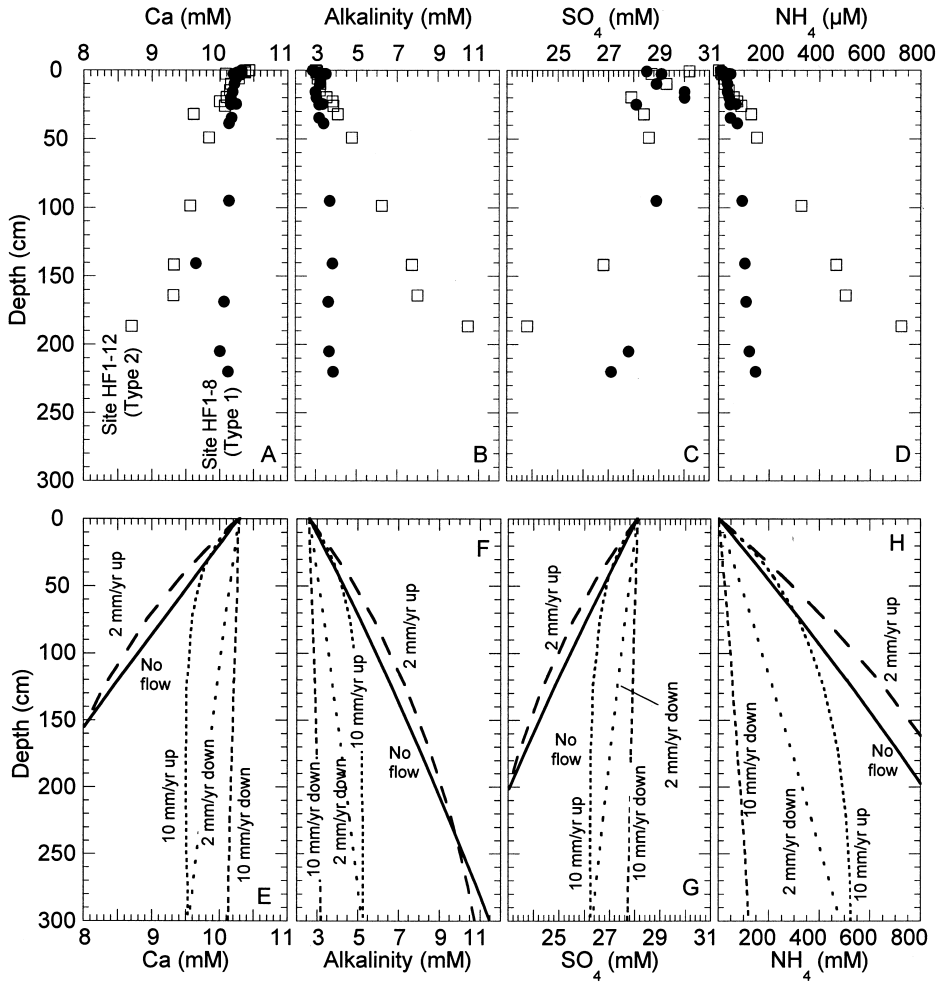

Fig. 5. Pore water concentrations from cores collected at two sites (HF1-8 and HF1-12) illustrating profile types, and reactive transport model results used to interpret the observations. Type 1 profiles are interpreted to indicate seawater recharge, and type 2 profiles are interpreted to indicate mainly diffusion and reaction. The distribution of type 1 and type 2 profiles is listed in Table 1. Example model results are based on the following conditions: basement temperature = 5°C; basement fluid = seawater; reactive TOC in the sediments = 1.5%; sedimentation rate = 0.06 mm/yr. Curves show modeled pore water profiles for various flow rates. Other boundary conditions and properties give somewhat different results, but the overall trends are the same, as described in the text. (A) Observed Ca. (B) Observed alkalinity. (C) Observed SO_4. (D) Observed NH_4. (E) Modeled Ca. (F) Modeled alkalinity. (G) Modeled SO_4. (H) Modeled NH_4.

able zone in upper basement, and appropriate fluid and sediment thermal properties, the data from 9–14 km from the ridge crest (Fig. 4A) suggest specific discharge of 2–3 m/yr. Assuming a thinner permeable zone requires a proportionately greater rate of discharge, as would thinner sediment cover. Some crustal heat is probably extracted by fluids flowing along strike, since depression of heat flow suggests that fluids enter basement on both sides of the trough, but limited observations do not allow us to map fluid pathways in detail at this time.

The mean heat flow deficit (the difference between lithospheric conductive and measured values, Fig. 4A) over the 11-km heat flow transect is 440 mW/m^2 ($\pm$100 mW/m^2, 1 S.D.). Integration along the transect results in a total heat deficit of 5 MW per kilometer of ridge crest. This heat output is equivalent to that of a single black smoker vent, and is similar to that estimated for combined focused and diffusive heat advection from the Baby Bare outcrop on the east flank of Juan de Fuca Ridge [30].

6.2. Geochemical analyses

We interpret sediment pore waters exhibiting little or no chemical difference from seawater (type 1) to indicate localized sites of downwelling, whereas sites with large geochemical gradients (type 2) are thought to indicate places where fluid–sediment reactions and diffusional processes dominate. We have run a set of numerical, reactive transport simulations to help place constraints on these interpretations. We used a modified version of GIMRT (Global Implicit Multicomponent Reactive Transport) [31] to conduct a series of one-dimensional simulations that incorporate sediment burial, fluid advection, species-specific molecular diffusion, organic matter degradation (via SO_4 reduction), and inorganic mineral diagenesis including calcite precipitation and dissolution. We focused on the influence of these reactions on pore water concentrations of Ca, alkalinity, SO_4, and NH_4 because these species showed the strongest contrast between the various sites and are particularly sensitive to organic matter degradation (Fig. 5). A conservative tracer such as chloride is commonly used for making seafloor seepage calculations based on pore fluids (e.g., [32,33]), but chloride concentrations did not vary significantly in the cores recovered from the flank of Alarcon Ridge. At the other extreme, biogenic silica was so abundant and highly reactive in Alarcon Basin sediments that it provides a relatively poor constraint on seepage rates.

All simulations were started with a 40-m-thick sediment layer having a constant porosity of 70%. Several sets of upper and lower boundary temperatures and fluid compositions were tested. At the upper boundary we used seawater chemistry and a bottom water temperature of 2°C. At the lower boundary, we tested three sets of conditions: seawater at 5°C, reacted basement fluid at 15°C, and reacted basement fluid at 20°C. The compositions we assumed for the reacted basement fluid were those of ODP Sites 1024 and 1025 (Juan de Fuca Ridge flank), with temperatures of 15°C and 20°C, respectively [34]. The sediment thermal gradient was held constant and conductive. Sediment was advected through the system at a constant sedimentation rate (values of 0.06–0.1 mm/yr were tested) and the models were run for 1.0–1.5 Myr, long enough to establish dynamic steady-state conditions. We also varied the quantity of reactive organic matter in the sediment column from 0.4 to 4.0%. We ran simulations that included no fluid flow through the sediments, and simulations with fluid seepage rates of 2 mm/yr up and down and 10 mm/yr up and down. All of these parameters influenced the modeled pore fluid profiles, several of which are compared to observational data (Fig. 5). Because of the wide range of free parameters, we did not attempt to 'best fit' model results to observations. Instead, we used the model results to suggest a range of conditions that are consistent with observations.

Type 1 profiles were most consistent with simulations that include downward seepage at rates on the order of 2–10 mm/yr. Upward seepage is much less efficient at suppressing pore water gradients unless velocities are considerably greater (Fig. 5), but higher upward velocities are inconsistent with heat flow profiles. Relatively slow seepage into the sediment was more consistent

with observations when we modeled the system with lower fractions of reactive OC (which result in a slower rates of SO_4 reduction) or with less reacted (and lower-temperature) basement fluid. Higher values for TOC or the extent of basement fluid reaction required higher downward seepage rates to match shallow pore water observations. Several combinations of TOC content, sedimentation rate, and basement fluid composition were also found to simulate type 2 profiles, but these profiles were best represented by simulations that included no fluid flow or very slow downflow (Fig. 5).

Vertical fluid flow can also influence conductive heat flow values (e.g., [11,35]), but curvature in thermal gradients due to fluid recharge is difficult to detect with a 3.5-m probe. Recharge at rates < 30 cm/yr would be rapid enough to produce a geochemical signal, but too slow to perturb shallow thermal gradients. Thus the geochemistry and heat flow data are entirely consistent with fluid recharge into the seafloor at rates on the order of 2–10 mm/yr.

We also note variations in chemical gradients with depth in Alarcon Basin sediments (Fig. 5). These variations could result from subtle differences in physical or chemical conditions with depth, transient or lateral fluid flow, or some combination of these conditions. More data and more comprehensive modeling will be required to test these possibilities and to evaluate differences in the location or intensity of pore fluid flow within shallow sediments.

6.3. Comparison to other sites

The hydrologic regime apparent in Alarcon Basin is similar to that documented on a sediment pond on 7.3 Ma crust on the west flank of the Mid-Atlantic Ridge (MAR) [29,36]. In that setting, elevated basement outcrops on either side of the sediment pond are thought to allow crustal-scale flow of seawater through basement. Heat flow in the MAR sediment pond is suppressed by 75–80% below that expected based on crustal age, and pop-up pore pressure instruments deployed within the sediment pond detected negative pressure gradients, indicative of slow seawater recharge [36,37]. Limited chemical analyses of sediment pore waters were also consistent with downward seepage of bottom seawater [38]. The interpretation that basement is underpressured below the sediment pond is consistent with the recharge of ocean bottom water for 17 years into DSDP Hole 395A, drilled through the edge of the pond and into the underlying basalt [39–41]. We suggest that hydrologic conditions responsible for fluid flow within young crust in Alarcon Basin are similar to those documented near DSDP Site 395.

Thermal, chemical, and hydrologic conditions east of Alarcon Ridge are also similar to those at other sites where young crust (< 1 Ma) created at an intermediate-rate spreading center is incompletely blanketed by sediments: the Galapagos Mounds field south of the Galapagos Spreading Center [15,42,43], and the west flank of the Juan de Fuca Ridge [16]. In these cases, mean heat flow is depressed significantly below that expected based on crustal age. However, heat flow measurements at each of these sites include scattered values considerably greater than predicted based on crustal age. These high values tend to be associated with the edges of abyssal hills, and have been interpreted to indicate localized fluid upflow along faults [16,42]. The Alarcon Basin data set is limited thus far, but we note only low heat flow values on the edges of the abyssal hills, and no evidence for hydrothermal discharge along hill-bounding faults or outcrops or through sediments.

7. Summary and conclusions

New seismic, heat flow, sediment and pore fluid geochemistry data from the east flank of Alarcon Ridge provide evidence for vigorous hydrothermal circulation within young oceanic crust formed at a moderate-rate spreading center. Heat flow values are 15–55% of that input at the base of the lithosphere for crust of this age. Heat flow is highest near the center of a sediment-filled trough, and lowest along the trough margins, suggesting that trough-bounding faults and basement exposures may help to focus hydrothermal recharge. Sediment and pore fluid geochemistry data, in

combination with reactive transport modeling, indicate that conditions within the shallow sediments are dominantly diffusive and reactive in two locations, but at other sites where cores were collected, the data suggest that bottom seawater recharges through the sediments at velocities of about 2–10 mm/yr. Seafloor heat flow appears to be entirely conductive, which is consistent with the low seepage velocities inferred from geochemical observations. The total fluid fluxes through sediments are probably small relative to direct basement recharge through basalt exposures, but recharge through sediments requires that basement is underpressured relative to local hydrostatic conditions.

Similar conditions have been detected on other young ridge flanks. A combination of heating from below, lateral and vertical differences in permeability, and basement relief and exposure results in vigorous fluid flow through basement, and slow recharge of seawater through overlying sediments. That conductive heat flow is consistently lower than that predicted based on crustal age requires that heat be removed advectively from basement. There are likely to be components of fluid flow moving across strike beneath the sediment-covered trough, and along strike of major tectonic structures. The heat flow deficit along the 11-km heat flow and coring transect in Alarcon Basin is 440 mW/m^2, equal to 5 MW per kilometer of ridge. This is equivalent to the combined advective and diffusive heat output through a single basement outcrop on the east flank of the Juan de Fuca Ridge. It seems likely that there are sites of diffuse and focused ridge flank discharge in Alarcon Basin. Careful surveys will help to locate fluid discharge areas in this area, and to assess the mechanisms by which heat and solutes are exchanged between the crust and ocean.

Acknowledgements

We are grateful for the advice and cooperation of colleagues from the Department of Geology at CICESE, Ensenada, Mexico, without whom the Alarcon Basin expedition would not have been possible. Gretchen Robertson and Holger Michaelis provided analytical assistance. We also thank SIO ship operations, and the officers and crew of the R/V *Roger Revelle*, particularly Capt. Chris Curl and Marine Technicians Seth Mogt and Bob Wilson. Funding in support of this project was provided by the UCSC Committee on Research, the CULAR/UCSC program (STB-UC 98-181), and NSF/OCE-9819242.***[EB]***

References

[1] H. Elderfield, A. Schultz, Mid-ocean ridge hydrothermal fluxes and the chemical composition of the ocean, Annu. Rev. Earth Planet. Sci. 24 (1996) 191–224.
[2] C. Stein, S. Stein, A model for the global variation in oceanic depth and heat flow with lithospheric age, Nature 359 (1992) 123–129.
[3] M.J. Mottl, C.G. Wheat, Hydrothermal circulation through mid-ocean ridge flanks: fluxes of heat and magnesium, Geochim. Cosmochim. Acta 58 (1994) 2225–2237.
[4] P. Lonsdale, Segmentation at disruption of the East Pacific Rise in the mouth of the Gulf of California, Mar. Geophys. Res. 17 (1995) 323–359.
[5] C. DeMets, A reappraisal of seafloor spreading lineations in the Gulf of California; implications for the transfer of Baja California to the Pacific Plate and estimates of Pacific-North America motion, Geophys. Res. Lett. 22 (1995) 3545–3548.
[6] T.H. van Andel, G.G. Shorr, Jr., Marine Geology of the Gulf of California Memoir 3, Am. Assoc. Petrol. Geol., Tulsa, OK, 1964.
[7] R. Larson, Bathymetry, magnetic anomalies, and plate tectonic history of the mouth of the Gulf of California, Geol. Soc. Am. Bull. 83 (1972) 3345–3360.
[8] R.P. Von Herzen, Geothermal heat flow in the Gulfs of California and Aden, Science 140 (1963) 1207–1208.
[9] L.A. Lawver, D. Williams, R.P. Von Herzen, A major geothermal anomaly in the Gulf of California, Nature 257 (1975) 23–28.
[10] P. Lonsdale, K. Becker, Hydrothermal plumes, hot springs, and conductive heat flow in the southern trough of Guaymas Basin, Earth Planet. Sci. Lett. 73 (1985) 211–225.
[11] A.T. Fisher, K. Becker, Heat flow, hydrothermal circulation and basalt intrusions in the Guaymas Basin, Gulf of California, Earth Planet. Sci. Lett. 103 (1991) 84–99.
[12] L. Lawver, D. Williams, Heat flow in the central Gulf of California, J. Geophys. Res. 84 (1979) 3465–3478.
[13] B.T.R. Lewis, Temperatures, heat flow, and lithospheric cooling at the mouth of the Gulf of California, in: B.T.R. Lewis, P. Robinson (Eds.), Init. Reports DSDP, 65, US Govt. Printing Office, Washington, DC, 1983, pp. 343–355.
[14] B.T.R. Lewis, W.E. Snydsman, J.S. McClain, M.L.

Holmes, C.R.B. Lister, Site survey results at the mouth of the Gulf of California, Leg 65, Deep Sea Drilling Project, in: B.T.R. Lewis, P. Robinson (Eds.), Init. Reports DSDP, 65, US Govt. Printing Office, Washington, DC, 1983, pp. 309–317.

[15] D.L. Williams, R.P. Von Herzen, J.G. Sclater, R.N. Anderson, The Galapagos Spreading Centre, lithospheric cooling and hydrothermal circulation, Geophys. J. R. Astron. Soc. 38 (1974) 587–608.

[16] H.P. Johnson, K. Becker, R.P.V. Herzen, Near-axis heat flow measurements on the northern Juan de Fuca Ridge: implications for fluid circulation in oceanic crust, Geophys. Res. Lett. 20 (1993) 1875–1878.

[17] F. Dunnebier, G. Blackinton, A man-made hot spring on the ocean floor, Nature 284 (1980) 338–340.

[18] R.D. Hyndman, E.E. Davis, J.A. Wright, The measurement of marine geothermal heat flow by a multipenetration probe with digital acoustic telemetry and in situ conductivity, Mar. Geophys. Res. 4 (1979) 181–205.

[19] E.E. Davis, C.R.B. Lister, J.C. Sclater, Toward determining the thermal state of old ocean lithosphere: heat flow measurements from the Blaka-Bahama Outer Ridge, Geophys. J. R. Astron. Soc. 78 (1984) 507–545.

[20] H. Villinger, E.E. Davis, A new reduction algorithm for marine heat-flow measurements, J. Geophys. Res. 92 (1987) 12,846–12,856.

[21] H. Villinger, E.E. Davis, HFRED: A Program for Reduction of Marine Heat Flow Data on a Microcomputer 1627, Geological Survey of Canada, Sydney, BC, 1987, 77 pp.

[22] A.E. Benfield, The effect of uplift and denudation on underground temperatures, J. Appl. Phys. 20 (1949) 66–70.

[23] M.G. Langseth, M.A. Hobart, K. Horai, Heat flow in the Bering Sea, J. Geophys. Res. 85 (B7) (1980) 3740–3750.

[24] L. Zühlsdorff, V. Spiess, C. Hübscher, M. Breitzke, Seismic reflectivity anomalies in sediments at the eastern flank of the Juan de Fuca Ridge, J. Geophys. Res. 104 (B7) (1999) 15351–15364.

[25] E.E. Davis, A.T. Fisher, J. Firth, Proceedings of the Ocean Drilling Program, Initial Reports 168, Ocean Drilling Program, College Station, TX, 1997, 470 pp.

[26] E. Giambalvo, A.T. Fisher, L. Darty, J.T. Martin, R.P. Lowell, Origin of elevated sediment permeability in a hydrothermal seepage zone, eastern flank of Juan de Fuca Ridge, and implications for transport of fluid and heat, J. Geophys. Res. 105 (B1) (2000) 913–928.

[27] A. Lachenbruch, Rapid estimation of the topographic disturbance to superficial thermal gradients, Rev. Geophys. Space Phys. 6 (1968) 365–400.

[28] M.G. Langseth, B. Herman, Heat transfer in the oceanic crust of the Brazil Basin, J. Geophys. Res. 86 (1981) 10805–10819.

[29] M.G. Langseth, R.D. Hyndman, K. Becker, S.H. Hickman, M.H. Salisbury, The hydrogeological regime of isolated sediment ponds in mid-oceanic ridges, in: R.H. Hyndman, M.H. Salisbury (Eds.), Init. Reports DSDP, 78B, US Govt. Printing Office, Washington, DC, 1984, pp. 825–837.

[30] M.J. Mottl, C.G. Wheat, E. Baker, N. Becker, E. Davis, R. Feeley, A. Grehan, D. Kadko, M. Lilley, G. Massoth, C. Moyer, F. Sansone, Warm springs discovered on 3.5 Ma oceanic crust, eastern flank of the Juan de Fuca Ridge, Geology 26 (1998) 51–54.

[31] C.I. Steefel, S.B. Yabusaki, OS3D/GIMRT, Software for Multicomponent-Multidimensional Reactive Transport, User Manual and Programmer's Guide, Pacific Northwest National Laboratory, Richland, WA, 1996.

[32] C.G. Wheat, M.J. Mottl, Hydrothermal circulation, Juan de Fuca Ridge eastern flank: factors controlling basement water composition, J. Geophys. Res. 99 (1994) 3067–3080.

[33] C.G. Wheat, R. McDuff, Mapping the fluid flow of the Mariana Mounds ridge-flank hydrothermal system: pore water chemical tracers, J. Geophys. Res. 100 (1995) 8115–8131.

[34] H. Elderfield, C.G. Wheat, M.J. Mottl, C. Monnin, B. Spiro, Fluid and geochemical transport through oceanic crust: a transect across the eastern flank of the Juan de Fuca Ridge, Earth Planet. Sci. Lett. 172 (1999) 151–165.

[35] J.D. Bredehoeft, I.S. Papadopulos, Rates of vertical groundwater movement estimated from the earths thermal profile, Water Resources Res. 1 (1965) 325–328.

[36] M.G. Langseth, K. Becker, R.P. Von Herzen, P. Schultheiss, Heat and fluid flux through sediment on the western flank of the Mid-Atlantic Ridge: a hydrogeological study of North Pond, Geophys. Res. Lett. 19 (1992) 517–520.

[37] W.W. Fang, M.G. Langseth, P.J. Schultheiss, Analysis and application of in situ pore pressure measurements in marine sediments, J. Geophys. Res. 98 (B5) (1993) 7921–7938.

[38] R. McDuff, The chemistry of interstitial waters from the upper oceanic crust, in: R.H. Hyndman, M.H. Salisbury (Eds.), Init. Reports DSDP, 78B, US Govt. Printing Office, Washington, DC, 1984, pp. 795–799.

[39] K. Becker, M.G. Langseth, R.D. Hyndman, Temperature measurements in Hole 395A, Leg 78B, in: R. Hyndman, M. Salisbury (Eds.), Init. Reports DSDP, 78B, US Govt. Printing Office, Washington, DC, 1984, pp. 689–698.

[40] R. Gable, R.H. Morin, K. Becker, Geothermal state of DSDP Holes 333A, 395A and 534A: Results from the dianaut program, Geophys. Res. Lett. 19 (1992) 505–508.

[41] K. Becker, M.J. Malone, Proc. ODP, Init. Reports 174B, Ocean Drilling Program, College Station, TX, 1998.

[42] D.L. Williams, K. Green, T.H. van Andel, R.P. Von Herzen, J.R. Dymond, K. Crane, The hydrothermal mounds of the Galapagos Rift: observations with DSRV Alvin and detailed heat flow studies, J. Geophys. Res. 84 (1979) 7467–7484.

[43] K.E. Green, R.P. Von Herzen, D.L. Williams, The Galapagos Spreading Center at 86°W: a detailed geothermal field study, J. Geophys. Res. 86 (B2) (1981) 979–986.